Solution Conformations of a Trimannoside from Nuclear Magnetic Resonance and Molecular Dynamics Simulations

Eric W. Sayers* and James H. Prestegard[†]

*Department of Pharmacology, Yale University, New Haven, Connecticut 06510, and [†]Complex Carbohydrate Research Center, University of Georgia, Athens, Georgia 30602 USA

ABSTRACT   N-linked oligosaccharides often act as ligands for receptor proteins in a variety of cell recognition processes. Knowledge of the solution conformations, as well as protein-bound conformations, of these oligosaccharides is required to understand these important interactions. In this paper we present a model for the solution conformations sampled by a simple trimannoside, methyl 3,6-di-O-(α-D-mannopyranosyl)-α-D-mannopyranoside, which contains two of the most commonly found glycosidic linkages in N-linked oligosaccharides. This model was derived from simulated annealing protocols incorporating distance restraints extracted from NOESY spectra along with torsional restraints computed from three-bond ^{1}H-^{13}C coupling constants measured across the glycosidic bonds. The model was refined in light of unrestrained molecular dynamics simulations conducted in the presence of solvent water. The resulting model depicts a molecule undergoing conformational averaging in solution, adopting four major and two minor conformations. The four major conformations arise from a pair of two-state transitions, one each at the $\alpha(1\rightarrow3)$ and $\alpha(1\rightarrow6)$ linkages, whereas the minor conformations result from an additional transition of the $\alpha(1\rightarrow6)$ linkage. Our data also suggest that the $\alpha(1\rightarrow3)$ transition is fast and changes the molecular shape slightly, whereas the $\alpha(1\rightarrow6)$ is much slower and alters the molecular shape dramatically.

INTRODUCTION

The interactions between proteins and oligosaccharides are essential to a number of important biological processes including cell-cell adhesion, cell recognition, and host defense (Drickamer, 1988; Lasky, 1992; Bevilacqua, 1993; Opdenakker et al., 1993; Gabius, 1997). Understanding these interactions must begin with a basic knowledge of the energetically allowed conformations of these molecules. The solution conformations of oligomannoses in particular have been studied for many years (Brisson and Carver, 1983a; Homans et al., 1986, 1987b), principally because these structures form the cores of the majority of N-linked oligosaccharides found in biology (Brisson and Carver, 1983b, 1983c). Particularly common are the $\alpha(1\rightarrow6)$ and $\alpha(1\rightarrow3)$ linkages, which find their most basic representation in the trimannoside studied here. We present in this paper a new and detailed study of the conformational distribution of methyl 3,6-di-O-(α-D-mannopyranosyl)-α-D-mannopyranoside. This molecule not only forms one of the most commonly observed branch points in N-linked oligosaccharides, but in some cases it also forms the terminus which is directly recognized by a protein-binding site, such as that in the rat mannose-binding protein, MBP-A (Weis et al., 1991, 1992).

To understand how the trimannoside is recognized by receptor proteins such as MBP-A, we need to understand not only its three-dimensional (3D) structure in solution but also the range of structures it adopts, and the relative populations of the individual structures. Solution NMR has proven to be a powerful tool in addressing the structures of oligosaccharides (van Halbeek, 1994), and indeed, this particular trimannoside has been previously studied by NMR (Brisson and Carver, 1983a). These authors reported that the molecule exists in two major solution conformations that differ only in the state of the ω dihedral angle of the $\alpha(1\rightarrow6)$ linkage. However, the significant technological advances in recent years, including high-resolution NOESY spectra, the ability to measure residual dipolar couplings in partially oriented liquid samples, and improved molecular dynamics (MD) force fields for carbohydrates, should well position us to extend our understanding of these important molecules. Here we present NOESY data, scalar coupling data, and MD simulations of this trimannoside with the goal of developing a model of its solution structure in terms of a small set of interconverting conformations. The resulting set of conformations can then be used as the basis for interpreting new types of data, such as those coming from measurements of residual dipolar couplings (Tian et al., 1999), and for elucidating the nature of oligosaccharide-binding to receptor proteins, such as mannose-binding protein (Bolon et al., 1999).

MATERIALS AND METHODS

Materials

Methyl 3,6-di-O-(α-D-mannopyranosyl)-α-D-mannopyranoside was obtained from BIOMOL Research Labs (Plymouth Meeting, PA) and was used without additional purification. The ring numbering system used in

this work is shown in Fig. 1 along with the nomenclature for the dihedral angles, which were defined according to IUPAC conventions (IUPAC−IUB, 1983): $\phi = O5(i) - C1(i) - On(i-1) - Cn(i-1)$, $\psi = C1(i) - On(i-1) - Cn(i-1) - C(n-1)(i-1)$, $\omega = O6(i) - C6(i) - C5(i) - C4(i)$, where i indicates a given residue and n a ring position.

NMR spectroscopy

NMR experiments described in this work were performed on one of the following instruments: a GE Omega spectrometer operating at a proton frequency of 500 MHz equipped with a Bruker triple-resonance, triple-axis gradient probe and an S-17 gradient accessory or a Varian UNITY-Plus spectrometer operating at a proton frequency of 600 MHz equipped with a triple-resonance HCN probe with z gradients. After collection, all data were processed using FELIX software (version 95.0, Biosym Technologies, San Diego, CA). All proton and ^{13}C chemical shifts are reported relative to internal DSS as previously outlined (Wishart et al., 1995).

All spectra of the free trimannoside were recorded at 25°C on a 20 mM sample in 0.5 ml of D_2O. ^{1}H-^{1}H DQF-COSY spectra were recorded on the Omega 500 using standard methods (Rance et al., 1983). Natural abundance ^{1}H-^{13}C heteronuclear single quantum coherence (HSQC) and heteronuclear multiple bond correlation (HMBC) spectra were recorded on the Varian 600 using pulsed field gradients to accomplish coherence selection (Bax and Summers, 1986; Davis et al., 1992; Tolman et al., 1992; Willker et al., 1993).

Selective 1D NOESY spectra were recorded on the Omega 500 using the double-pulsed field gradient sculpted excitation (DPFGSE) NOESY experiment (Stott et al., 1995). The proton offset was positioned on the proton of interest, and selective excitation was achieved by using 19.0-ms hyperbolic secant pulses. A total of 4096 complex points were acquired using a spectral width of 2500 Hz, yielding an acquisition time of 1.64 s. Along with the pre-delay of 2.0 s, this generated a total recycle time of 3.64 s. A total of 128 scans was acquired for each mixing time (300–1200 ms), and the data were apodized with a Kaiser window before Fourier transformation.

EXSIDE spectra were recorded on the Omega 500 as described in the literature for the measurement of transglycosidic coupling constants, $^{3}J_{CH}$ (Krishnamurthy, 1996). The spectral width in the direct dimension was 2500 Hz, and 48 scans were acquired for each free induction decay (FID) of 512 complex points. The spectral width in the indirect dimension was 3750 Hz, and 370 complex points were collected using gradient coherence selection. The proton and ^{13}C offsets were set at 4.90 and 67.5 ppm, respectively. Selective excitation was achieved using 8.0-ms G3 Gaussian cascades (Emsley and Bodenhausen, 1990). Before Fourier transformation,
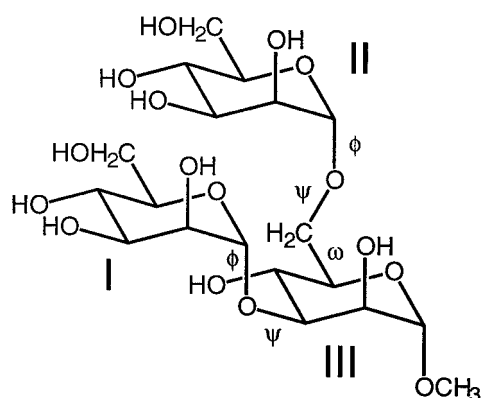

FIGURE 1   Structure of methyl 3,6-di-O-(α-D-mannopyranosyl)-α-D-mannopyranoside. Rings are labeled by roman numerals, and glycosidic dihedral angles are labeled ϕ, ψ, and ω.

each direct dimension FID was apodized with a Kaiser window and zero-filled to 1024 points. Each indirect FID was apodized with a 90°-shifted squared sinebell window and zero-filled to 512 points, yielding a 1024×512 matrix.

Simulation of NMR data

To analyze properly the intensities generated in NOESY spectra of strongly coupled spin systems, multiplet simulations were performed. An SGI INDY workstation (Silicon Graphics, Mountain View, CA) equipped with a 150-MHz R4400 processor was used along with GAMMA 3.5 software (Smith et al., 1994). The simulated spin system consisted of five spins corresponding to I-H1, III-H3, III-H4, III-H2, and III-H5. Coordinates of these spins were taken from the PDB file of a selected minimized structure, and chemical shifts and coupling constants were taken from Table 1. The correlation time for all spins was set to 100 ps, and full relaxation matrices were calculated under the influence of dipolar relaxation and J coupling. The frequency offset was set at 4.50 ppm, and each resulting FID contained 1024 complex points over a spectral width of 1000 Hz. The simulated experiment consisted of a selective 180° pulse at the offset followed by a mixing time of 600 ms, followed by a 90° pulse and acquisition. Two such FIDs were produced, one in which the selective pulse was applied and one in which it was not. The two FIDs were subtracted, zero-filled to 4096 points, and apodized using a Kaiser window before Fourier transformation. Each FID required ~12 h of computing time.

Analysis of NMR data

After Fourier transformation, DPFGSE NOE spectra were first baseline corrected using third-order polynomials, and all peaks were integrated. The integrated intensities of the auto peaks of a given spin were plotted as a function of the mixing time, τ, and extrapolated to $\tau = 0$ to derive M_0, the equilibrium magnetization for that spin. The integrated intensities of the cross-relaxation peaks were also plotted versus τ as fractions of M_0, and these plots were fitted to Eq. 1 using KaleidaGraph 3.0.2 (Abelbeck Software).

$$I_c(\tau) = c_1 + c_2\tau \exp(-c_3\tau) \tag{1}$$

In this expression, c_1 is an offset parameter, $c_2 \propto \sigma$, the cross-relaxation rate constant, and $c_3 = 1/T_1$. Distance restraints were derived from these data using the following expression:

$$r_{exp} = (c_{2ref}/c_{2exp})^{1/6} r_{ref} \tag{2}$$

where r_{exp} is the unknown distance between a given spin pair, r_{ref} is a known distance between a separate spin pair, and c_{2ref} and c_{2exp} are the parameters in Eq. 1 corresponding to the two spin pairs. For restraints involving methyl protons, c_{2exp} was first corrected to account for the degeneracy of these protons (Heatley et al., 1980; Oswood et al., 1997). In the present work, we used the distances and buildup rates of the intra-ring NOESY peaks between the anomeric proton and H2 of each ring as r_{ref} and c_{2ref}, assuming that these distances are fixed and well known. In addition, we converted the error in the buildup rate from the curve fitting (δc_2) to an error in the corresponding distance (δr) using standard formulas for propagation of error.

Computational methods

All minimizations, simulated annealing procedures, and MD simulations were performed using AMBER 4.1 (Pearlman et al., 1995) supplemented by the GLYCAM parameter set (Woods et al., 1995) on a Silicon Graphics Origin 200 workstation equipped with two 180-MHz R10000 processors. Files for the GLYCAM_93 parameter set were downloaded from http://

TABLE 1 Chemical shift assignments (ppm) and $^3J_{HH}$ values (Hz) of the trimannoside

Position	Ring I		Ring II		Ring III	
	^{1}H	^{13}C	^{1}H	^{13}C	^{1}H	^{13}C
1	5.09 (1.8)	103.3	4.90 (1.6)	100.0	4.72 (1.8)	101.7
2	4.06 (3.6)	70.6	3.98 (3.3)	70.4	4.08 (3.3)	70.0
3	3.87 (9.5)	71.0	3.83 (8.8)	71.2	3.85 (9.5)	79.2
4	3.65 (8.0)	67.3	3.64 (10.3)	67.3	3.88 (9.8)	66.2
5	3.75 (mm, de)	73.9	3.69 (2.3, 5.4)	73.3	3.79 (4.2, 2.2)	71.5
6, 6′	3.88, 3.75 nm	61.5	3.88, 3.75 (12.4)	61.5	4.00R, 3.73S (11.3)	65.8
OCH$_3$					3.40	55.4

Values in parentheses are $^3J_{HH}$ values measured from DQF-COSY data between proton i and $i + 1$, where i is the indicated position. For position 5, the two values correspond to couplings from H5 to H6 and H6′, respectively. For position 6, 6′, the value corresponds to the geminal coupling between H6 and H6′. nm, coupling was not measured due to spectral overlap; de, coupling was not observable because spins were degenerate.

www.amber.ucsf.edu/amber/ff94_glycam.html, whereas files for the GLYCAM_97a set were generously provided by Robert Woods. Molecular structures were viewed and manipulated using MidasPlus (Ferrin et al., 1988). For all in vacuo simulations, AMBER was configured for the 1991 AMBER force field supplemented by the GLYCAM 93 parameter set. For simulations including TIP3P water, AMBER was configured for the 1994 AMBER force field supplemented by the GLYCAM 97a parameter set.

Penalty functions for both distance and torsional restraints are implemented in AMBER as flat-bottomed wells with sides described by a hybrid harmonic-linear function. The function is flat between two values, $r2$ and $r3$, beyond which the walls are parabolic from $r2$ to $r1$ and from $r3$ to $r4$. The parabolas below $r2$ and above $r3$ are defined by force constants $rk2$ and $rk3$, respectively. Below $r1$ and above $r4$ the function is linear. For positive distance restraints derived from NOESY data, $r1$ and $r4$ were set to 1.80 Å and 3.50 Å, respectively, for all target distances r_0, thereby causing the slope of the function for $r > r4$ to decrease as r_0 increases, paralleling the reduced precision of the NOE at large internuclear distances. Parameters $r2$ and $r3$ were set, respectively, to $(r_0 - \delta r)$ and $(r_0 + \delta r)$, where δr is the error in the target distance described above. For restraints involving methyl protons, the distance r was measured from the arithmetic average position of the three methyl protons. Force constants $rk2$ and $rk3$ were set to 10 kcal/mole-Å^2. For all positive restraints, a distance r was considered to violate the restraint if $r < r1$ or if $r > r3 + 0.5$ Å. Restraints corresponding to a failure to observe a NOESY connectivity were used sparingly. For these negative restraints, parameters were set as follows: $r1 = 3.00$ Å, $r2 = r3 = 4.00$ Å, $r4 = 5.00$ Å. The force constant $rk2$ was set to 10 kcal/mole-Å^2, while $rk3$ was set to zero. A distance r was considered to violate these restraints only if $r < r1$.

Torsional restraints derived from $^3J_{CH}$ measurements were parameterized directly from the Karplus relationship (Tvaroska et al., 1989):

$$J = 5.7 \cos^2\phi_H - 0.6 \cos \phi_H + 0.5 \qquad (3)$$

In this equation, ϕ_H was defined as H1(i) − C1(i) − On(i − 1) − Cn(i − 1), so that $\phi = \phi_H + 120°$, where ϕ is defined according to IUPAC convention as described above. This equation was supplied to AMBER, which then calculated J values continuously during the simulations for each specified dihedral angle, ϕ_H. Parameters for these restraints were set as follows: $r1 = J - 2(\delta J)$, $r2 = J - \delta J$, $r3 = J + \delta J$, and $r4 = J + 2(\delta J)$, where δJ is the error in the measurement of J (0.4 Hz). Force constants $rk2$ and $rk3$ were set to 10 kcal/mol-rad^2. Two additional types of angular restraints were used. First, as discussed below, II-III ω was restrained to values between 60° and 180° based on earlier results (De Bruyn and Anteunis, 1976) as follows: $r1 = 40°$, $r2 = 50°$, $r3 = 190°$, and $r4 = 200°$. Secondly, the ring restraints used to lock the pyranose rings into chair conformations were set as follows: $r1 = \alpha - 20°$, $r2 = \alpha - 10°$, $r3 = \alpha + 10°$, and $r4 = \alpha + 20°$, where α values were measured from a minimized pyranose ring. Force constants $rk2$ and $rk3$ for these two types

of restraints were set to 100 kcal/mol-rad^2. A torsion ϕ was considered to violate the restraint if $J < r1$ or $J > r4$ for restraints based on J couplings calculated using Eq. 3, or if $\phi < r1$ or $\phi > r4$ for restraints defined in angular units ranging from 0° to 360°.

Simulated annealing procedures were performed in vacuo using the SANDER module of AMBER. The presence of water was simulated by a distance-dependent dielectric and the temperature was controlled by the temperature coupling algorithm of Berendsen et al. (1984). The SHAKE algorithm was used to constrain bond lengths, and the initial velocities were computed from a Maxwellian distribution at 10 K. The time step for all runs was 1 fs, and the nonbonded pair list was updated every 25 fs. All runs began with the same initial structure, which was constructed using MacroModel 3.5a (Mohamadi et al., 1990), and then minimized as described below. Beginning at 10 K, the system was heated to 5000 K in 1.0 ps and was maintained at 5000 K for 10 ps. The system was then cooled to 500 K in 10 ps, then to 300 K in 4 ps, and then to 10 K in 30 ps. Finally, the system was maintained at 5 K for 1 ps. This resulted in a total simulation time of 56 ps. Restraints derived from NOESY and J coupling data, along with the torsional restraint for II-III ω, were applied at the end of the heating period and were maintained for the remainder of the simulation. Dihedral angle restraints for the pyranose ring atoms were applied for the entire simulation, including the heating period. Each structure required ~90 s of computing time. Each of the resulting structures was then minimized in vacuo without restraints using the conjugate gradient method with a 10-Å cutoff for nonbonded interactions. In these minimizations, the presence of water was simulated by a distance-dependent dielectric. These minimizations proceeded until the RMS deviations were less than 0.0001 kcal/mol-Å, which generally occurred after 10,000–20,000 steps.

Molecular dynamics simulations were conducted to allow us to assess the effects of dynamic averaging on the mean values of restrained distances and torsions. These simulations were performed on a model including a single molecule of the trimannoside immersed in a bath of TIP3P water. Water molecules were initially placed throughout a region reaching out to 10 Å from trimannoside atoms with no water oxygen or hydrogen atoms approaching a trimannoside atom at distances less than 2.8 Å and 2.3 Å, respectively. This produced a 35.3 × 27.8 × 26.3 Å solvent box containing 676 water molecules solvating the sugar. This model was then minimized for 1000 steps in a constant dielectric using the steepest descent method with a 10-Å cutoff for nonbonded interactions. The system was then subjected to 1 ns of unrestrained MD at 300 K under constant pressure conditions of 1 atm using a 1-fs time step. A constant dielectric was used, and scaling factors of 0.2 ps were used in the Berendsen algorithm for the ligand and solvent. The SHAKE algorithm was used to constrain bond lengths, and initial velocities were calculated from a Maxwellian distribution at 10 K. The cutoff for nonbonded interactions was set to 8.0 Å, and the nonbonded pair list was updated every 25 fs. During the course of the run, coordinates and energy statistics were output every 250 fs.

Grid searches were used to interpret proton-proton distances about the I-III glycosidic linkage in terms of I-III ϕ and ψ. These were performed using in-house software. Arrays of internuclear distances d(I-H1, III-H3), d(I-H1, III-H4), and d(III-H2, I-H5) at various values of I-III ϕ and ψ were obtained from Insight II (v. 98.0) modeling software (Molecular Simulations, San Diego, CA). For each distance, a fifth-order two-variable polynomial function, $r_{ij} = f_{ij}(\phi, \psi)$, was fit to the corresponding array of points, and these functions were then used to compute internuclear distances for arbitrary values of ϕ and ψ. Normally distributed populations of ϕ and ψ ($n = 1000$) were produced using the Box-Muller method (Press et al., 1992). The step sizes for these searches were as follows: for the dihedral angle means, 10°; for the standard deviations of the normal distributions, 3–5°; and for the fractional populations of each normally distributed set, 0.05 on a scale of 0.0–1.0.

RESULTS

Chemical shift assignment of the trimannoside

A DQF-COSY spectrum was able to provide unambiguous assignments for all protons except H5, H6, and H6′ of rings I and II. The stereospecific assignment of the two methylene protons attached to III-C6 was completed by comparing the relative magnitudes of the J couplings between H5 and these two methylene protons along with NOE-derived distance restraints (De Bruyn and Anteunis, 1976; Rao and Perlin, 1983). The assignment of all proton and ^{13}C spins was completed through the use of ^1H-^{13}C HSQC and HMBC spectra. The final assignments are listed in Table 1. These assignments agree with those reported for a disaccharide corresponding to the trimannoside in the present study without ring I (Spronk et al., 1995). Homonuclear proton $^3J_{HH}$ couplings obtained from the DQF-COSY spectrum are listed in Table 1.

Collection of distance restraints

Distance restraints were collected by quantitating the buildup of cross-relaxation observed in selective 1D DPFGSE NOE experiments (Fig. 2). Based on their spectral resolution, we chose to excite the three anomeric protons along with two pairs of spins that could be selectively excited together: III-H2, I-H2 and III-H6R, II-H2. In all
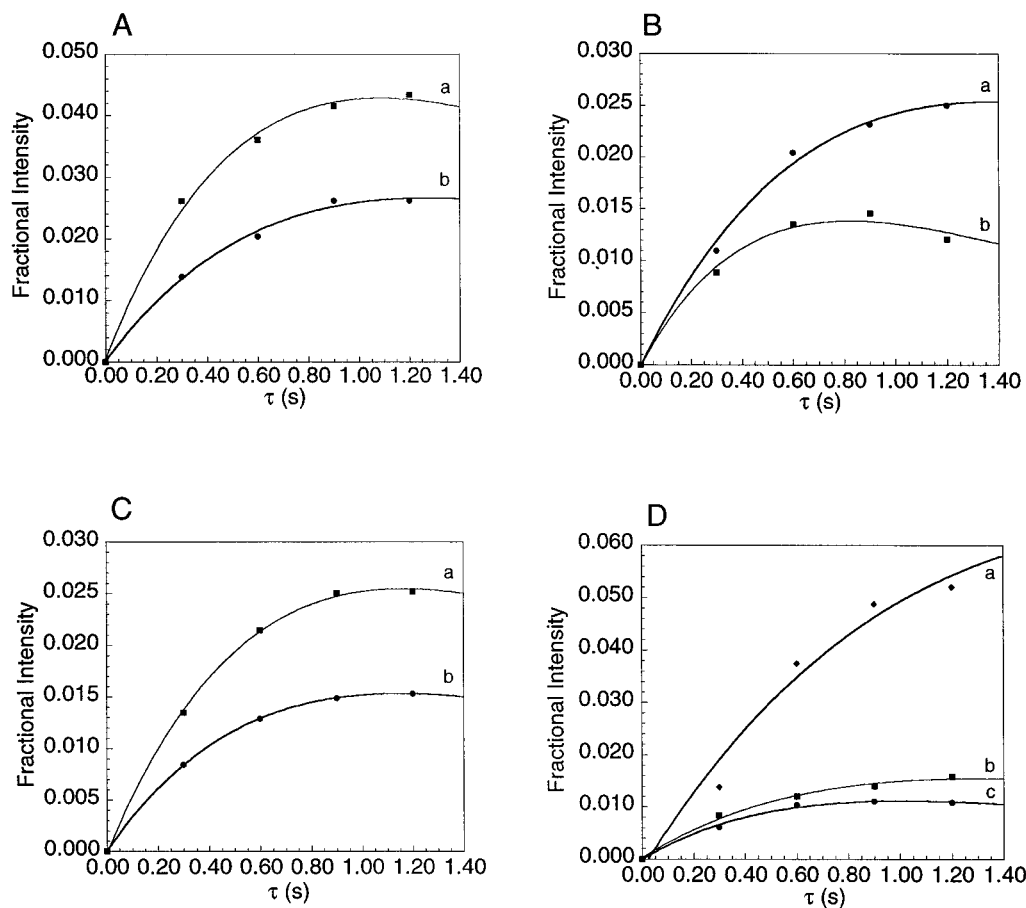

FIGURE 2 Buildup curves obtained from DPFGSE NOESY experiments. All intensities are reported as fractional intensities of the auto peak of the inverted spin at $\tau = 0$. (*A*) Inversion of I-H1; intensities of cross-peaks to III-H3/III-H4 (*a*) and I-H2 (*b*). (*B*) Inversion of II-H1; intensities of cross-peaks to II-H2 (*a*) and III-H6S (*b*). (*C*) Inversion of III-H1; intensities of cross-peaks to OCH$_3$ (*a*) and III-H2 (*b*). (*D*) Inversion of III-H2; intensities of cross-peaks to III-H3 (*a*), III-H1 (*b*), and I-H5 (*c*).

cases, dipolar connectivities revealed by these 1D experiments were confirmed by examining a conventional 2D NOESY spectrum. The assignment of the cross-relaxation peaks was straightforward for III-H1 (III-H2 at 4.08, OCH$_3$ at 3.40) and II-H1 (II-H2 at 3.98, III-H6S at 3.73). In one case the absence of an NOE was deemed significant, in that no NOE was observed between II-H1 and III-H6R. As these two protons are very close in space in many conformations of the $\alpha(1\rightarrow6)$ glycosidic linkage, the lack of this NOE imparted significant limits on the allowed conformations.

The assignment of the cross-peaks resulting from exciting III-H2 was somewhat more complicated due to degeneracy at the frequency of one of the observed cross-peaks. Three cross-peaks were observed, and two were readily assigned to III-H1 and III-H3. However, three spins (I-H5, I-H6′, and II-H6′) resonate at 3.75 ppm, the position of the third cross-peak, a 9-Hz doublet. Based on model building, only I-H5 and I-H6′ can approach III-H2 within 4.0 Å. Of these two spins, only I-H5 should give the observed 9-Hz doublet based on the J couplings in Table 1. Therefore, this cross-peak was assigned to I-H5.

We encountered similar complications in assigning the cross-peaks resulting from exciting I-H1. Two cross-peaks were observed, one of which was readily assigned to I-H2. The second cross-peak was a complex multiplet stretching from 3.83 to 3.88 ppm, an area in which six spins (II-H3, III-H3, I-H3, I-H6, II-H6, and III-H4) resonate. Based on model building, only III-H3 and III-H4 are able to approach I-H1 within 4.0 Å without significant steric strain. However, neither alone should have produced a complex multiplet, so we had to consider the possibility of NOE transfer to both spins. Modeling suggested that a simultaneous NOE from I-H1 to both III-H3 and III-H4 was possible. The data in Table 1 show that these two spins differ in chemical shift by only 15 Hz (at 500 MHz) and are involved in a coupling of 10 Hz. Thus, we also had to consider transfers to this complex multiplet due to second-order effects. We attempted to resolve the contributions from these mechanisms by simulating the 1D NOESY spectrum arising from selective inversion of I-H1 using GAMMA 3.5 software (Smith et al., 1994). Two simulations were performed: one to simulate the amount of cross-relaxation between I-H1 and III-H4 that was expected from a reasonable low-energy structure of the trimannoside consistent with the other experimental restraints and a second to simulate the absence of cross-relaxation between I-H1 and III-H4. Both incorporated I-H1 to III-H3 direct cross-relaxation interactions. The first simulation used coordinates from a structure in which the distances from I-H1 to III-H3 and III-H4 were 2.79 Å and 3.43 Å, respectively, which should have generated a NOESY intensity distribution of ~70/30 between III-H3 and III-H4. The second used the same coordinates, except that the x-coordinate of III-H4 was increased by 10,000 Å, which should have resulted in 100% of the NOESY intensity at III-H4 arising from strong coupling to III-H3. The

results of these simulations along with the experimental data are shown in Fig. 3. Also shown is a 1D proton spectrum of the trimannoside for comparison. It is clear from the figure that the simulated multiplets bracket the experimental spectrum with respect to the intensity of the III-H4 multiplet. This suggested that at least a small amount of cross-relaxation was occurring directly between I-H1 and III-H4 and that the NOESY intensity distribution between III-H3 and III-H4 lay between 70/30 and 100/0. We therefore constructed distance restraints for III-H3 and III-H4 in which
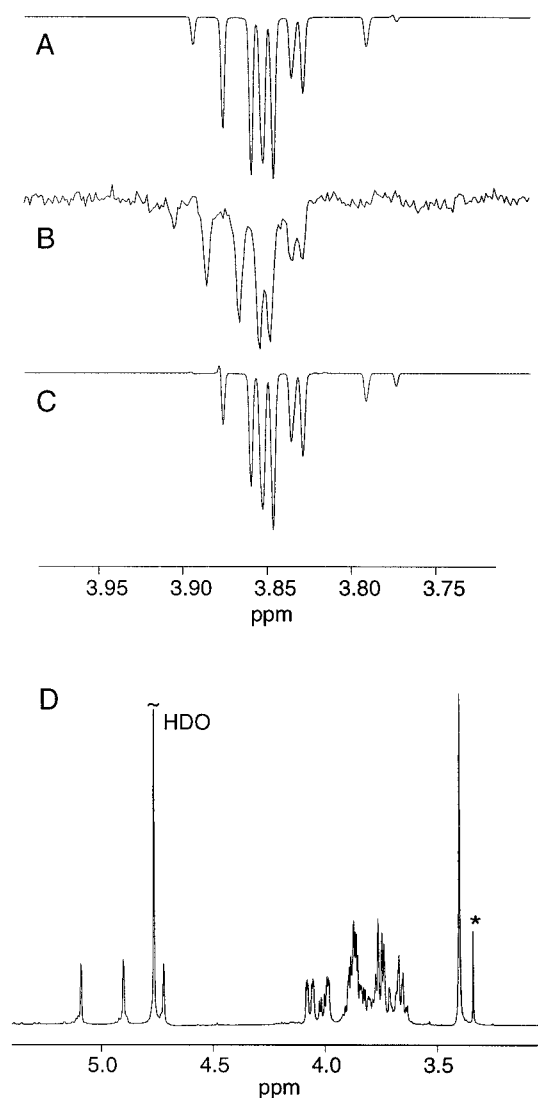

FIGURE 3 Simulated multiplets for the III-H3/III-H4 spin pair. (*A*) Simulated multiplet for a system corresponding to a minimized structure of the trimannoside in which d(I-H1/III-H3) = 2.79 Å and d(I-H1/III-H4) = 3.43 Å. (*B*) Portion of the DPFGSE NOESY spectrum upon inversion of I-H1 with a mixing time of 600 ms. (*C*) Simulated multiplet for a system in which III-H4 is placed 10,000 Å from I-H1 and d(I-H1/III-H3) = 2.79 Å. (*D*) One-dimensional 500-MHz proton spectrum of the trimannoside. The small peak marked with an asterisk corresponds to residual methanol from the commercial preparation.

the limits of the flat bottom of the energy well were set to distances that should generate NOESY intensity distributions of 90/10 and 70/30. Otherwise, these restraints were constructed as described in Materials and Methods. The final set of distance restraints derived from NOESY data is listed in Table 2.

Collection of torsional restraints

Torsional restraints for the ϕ dihedral angle of the glycosidic linkages were derived by measuring the three-bond $^1H1\text{-}C1\text{-}On\text{-}^{13}Cn$ heteronuclear J couplings using the EXSIDE experiment (Krishnamurthy, 1996; Rundlof et al., 1998; Otter et al., 1999). This experiment is attractive because it allows these couplings to be measured in a single spectrum directly from in-phase multiplets free of contamination from proton homonuclear couplings as encountered in many other methods. The method achieves this by selectively inverting a set of proton spins that have similar chemical shifts but are not scalar coupled to one another. In the case of the trimannoside, the anomeric spins were excellent candidates (Fig. 3 D). Measuring couplings that report on the ψ dihedral angle was much less straightforward as a similar set of ring protons would have needed to be inverted selectively, which was impossible given the overlap in that spectral region. The J couplings measured across the glycosidic linkage are shown in Table 3, along with the $^1H1\text{-}C1\text{-}O5\text{-}^{13}C5$ couplings as controls and their corresponding angular values according to Eq. 3. Because the H1-C1-O5-C5 dihedral angle is fixed near 180° by the pyranose ring geometry, the H1-C5 three-bond coupling should have a value of ~6 Hz according to Eq. 3, and this is confirmed by the data.

The remaining torsion of structural interest is the ω dihedral angle of the $\alpha(1\rightarrow6)$ linkage between rings II and III. Although this torsion normally adopts one of three low-energy states (60°, 180°, −60°), it has been known for some time that due to steric clashes between OH4 and OH6, among other factors, the $\omega = -60°$ rotamer is not significantly populated in pyranose rings of D-glucose or D-man-

TABLE 2 Results of fitting NOESY buildup data to Eq. 1

Proton pair	c_2	δc_2	r (Å)	δr
I-H1, I-H2	0.0565	0.00567	2.52	
I-H1, III-H3	0.0848*	0.00737	2.36	0.05[†]
I-H1, III-H4	0.0212*	0.00184	2.97	0.20[‡]
II-H1, II-H2	0.0505	0.00572	2.51	
II-H1, III-H6S	0.0465	0.00596	2.54	0.07
III-H1, III-H2	0.0362	0.000273	2.54	
III-H1, OCH3	0.0600	0.00226	2.80[§]	0.02
III-H2, I-H5	0.0299	0.00319	2.62	0.05

*Corresponds to an 80/20 intensity distribution as described in the text.
[†]Well bottom: r2 = 2.26; r3 = 2.46.
[‡]Well bottom: r2 = 2.71; r3 = 3.40.
[§]Corrected for the degeneracy of the methyl protons.

TABLE 3 $^3J_{CH}$ values (Hz) measured from EXSIDE data and corresponding dihedral angle states

^1H	^{13}C	$^3J_{CH}$	(ϕ_1, ϕ_u)*
I-H1	I-C5	6.2	*(−169, −156), (156, 169)*
I-H1	III-C3	2.4	(166, 175), **(65, 74)**, (−122, −114), (−6, 2)
II-H1	II-C5	6.1	*(−167, −155), (155, 167)*
II-H1	III-C6	1.6	(175, 186), **(54, 65)**, (−132, −122), (2, 12)
III-H1	III-C5	6.0	*(−165, −153), (153, 165)*
III-H1	OCH3	2.5	(165, 174), **(66, 75)**, (−121, −113), (−7, 1)

*Sets of dihedral angle values in degrees consistent with torsional restraint parameters ($r2 = J - \delta J$, $r3 = J + \delta J$) calculated according to Eq. 3, with $\delta J = 0.4$ Hz. Values in bold lie closest to the ϕ states that were sampled in simulated annealing and MD simulations. Values in italics are ϕ_H angles for H1-C1-O5-C5 torsions and are listed for validation purposes only.

nose (De Bruyn and Anteunis, 1976). The values of the proton $^3J_{HH}$ couplings between H5 and the exocyclic methylene protons (H6R, H6S) discussed above, along with the chemical shifts of these protons, are consistent with previous work (Rao and Perlin, 1983), and thus ω was restrained to values between 60° and 180° as described in Materials and Methods.

Simulated annealing

Our initial goal was to develop a reliable heating segment at the beginning of the simulated annealing protocol, as other authors had reported that a variety of ring deformations, including boat and skewed chair conformations, were produced during this segment (Rutherford et al., 1993; Rutherford and Homans, 1994; Renouf and Hounsell, 1995). We initially used heating segments at the relatively low temperature of 750 K without any restraints, and indeed, we found that approximately half of the resulting structures contained one or more rings in a distorted geometry. We remedied this problem by incorporating strong torsional restraints (force constants of 100 kcal/mol-rad^2) for the pyranose ring itself (Renouf and Hounsell, 1995). Restraints based on a minimized chair conformation were applied to the four ring dihedral angles of each ring in the trimannoside (C1-C2-C3-C4, C2-C3-C4-C5, C3-C4-C5-O5, and C4-C5-O5-C1), giving a total of 12 restraints. Including these restraints completely eliminated all distorted ring conformations, even at 5000 K. In addition, although only two of the six glycosidic dihedral angles sampled all 360° of torsional space at the end of a 750 K heating segment (with the remaining four sampling between 50° and 200°), four of these six dihedral angles sampled all 360° at the end of a 5000 K heating segment (with the remaining two sampling between 180° and 300°). We therefore employed a heating segment at 5000 K for all subsequent calculations.

We first calculated an ensemble of 10 structures, ensemble A, using the restraints listed in Tables 2 and 3. After minimization, the members of this ensemble adopted one of three conformations (A1, A2, or A3), which differed only in

the ϕ and ψ torsions of the II-III linkage and the OCH$_3$ ϕ torsion. Tables containing detailed parameter statistics of these conformations may be found at http://tesla.ccrc. uga.edu/supplements. None of the structures contained violations of either distance or torsional restraints after simulated annealing; however, after minimization during which restraints were not applied, several restraint violations appeared. Structures adopting conformations A2 and A3 placed II-III ϕ at 150.60 ± 1.76° and 169.87 ± 0.03°, respectively, and both of these values violate the torsional restraint on this dihedral angle (Table 3). Conformation A3 placed OCH$_3$ ϕ at 148.67 ± 0.22°, which also violates the corresponding restraint. In addition, although some individual structures proved acceptable, the average values of I-III ϕ for the three minimized conformations (55.48°, 54.09°, and 57.08° for A1, A2, and A3, respectively) all violated the restraint for that torsion. One conformation, A2, also violated the negative d(II-H1, III-H6R) restraint by placing this distance at 2.37 ± 0.00 Å. Conformation A1 proved the most acceptable, with the fewest violations on average after minimization, and it was also at least 3 kcal/mol lower in energy than A2 and A3. However, when we generated a list of all proton pairs in A1 whose internuclear distance was less than 4.00 Å, two proton pairs emerged that are not listed in Table 2: I-H5/III-H3 and II-H1/III-H5. A NOESY cross-peak connecting I-H5 and III-H3 would appear at (3.75, 3.85) ppm, which is very close to the intense cross-peaks at (3.75, 3.88) ppm between I-H6 and I-H6′ and between II-H6 and II-H6′. Hence, it may have been obscured. The absence of the II-H1/III-H5 cross-peak at (4.90, 3.79) ppm, which would have been well separated from all other cross-peaks, could not be dismissed. We thus concluded that conformation A1 was also flawed and therefore introduced an additional negative distance restraint between II-H1 and III-H5 in a second round of simulated annealing.

Using the modified restraint set including the negative d(II-H1, III-H5) restraint, we calculated a second ensemble of 30 structures, ensemble B. After minimization, the members of ensemble B could be grouped into seven conformations (Table 4). B1 is equivalent to A1 except at II-III ψ, the latter of which placed this torsion at 70.25 ± 0.36°. Modeling easily showed that the shift from 70° in A1 to 180° in B1 can be directly attributed to the influence of the negative d(II-H1, III-H5) restraint, which is not violated by any structure in ensemble B. B2 differs from B1 only at II-III ω, and together these conformations account for 13 of the 30 structures. B3 and B7 are simply reproductions of A2 and A3, respectively. This leaves three new conformations produced in ensemble B: B4, B5, and B6. B4 is equivalent to B1 except at OCH$_3$ ϕ. B5 and B6 both have a II-III ω value near 60° and thus can be considered to be variations of B2 much as B3 and B7 are variations of B1 (II-III ω = 180°). As observed before, none of the structures contained violations after simulated annealing, but several violations appeared when these structures were minimized. Of the several conformations, B1 and B2 proved the most acceptable in terms of low energies and minimal numbers of violations. However, with II-III ψ at 180°, they did violate the negative d(II-H1, III-H6R) restraint by placing this distance at 2.94 ± 0.01 Å and 2.88 ± 0.05 Å, respectively. Taken together, the results of simulated annealing suggested that a single state of I-III ϕ, I-III ψ, and II-III ψ may simply be unable to satisfy all of the restraints simultaneously. To investigate this question further, we next turned to a more

TABLE 4 Glycosidic dihedral angles in conformations generated in ensemble B

Conformation	Energy Min*	I-III ϕ		I-III ψ		II-III ϕ		II-III ψ		II-III ω		OCH$_3$ ϕ	
		SA[†]	Min[‡]	SA	Min	SA	Min	SA	Min	SA	Min	SA	Min
B1[§]	5.150	64.62	59.34[¶]	−154.49	−158.25	53.55	64.01	159.24	−172.34	−176.72	−179.64	65.82	63.53
(8)	(0.702)	(0.25)	(6.53)	(1.71)	(13.27)	(0.23)	(0.20)	(1.86)	(0.33)	(3.03)	(0.47)	(0.19)	(0.13)
B2	5.027	64.53	59.14[¶]	−154.65	−159.36	53.78	66.09	140.28	−171.30	62.29	60.26	65.92	64.35
(5)	(0.809)	(0.06)	(4.77)	(1.85)	(9.86)	(0.28)	(1.68)	(5.65)	(2.67)	(2.67)	(1.00)	(0.12)	(0.13)
B3	7.763	76.64	65.39	−156.22	−146.36	179.74	*149.18*	102.58	−178.91	−175.18	179.94	73.81	63.25
(9)	(0.941)	(33.28)	(4.25)	(16.53)	(8.47)	(1.16)	*(1.10)*	(0.87)	(0.42)	(1.15)	(0.27)	(2.46)	(0.11)
B4	7.918	64.65	*55.00*	−155.04	−167.25	53.40	63.84	159.32	−173.09	−178.11	−179.86	165.12	*149.75*
(3)	(0.234)	(0.10)	*(3.87)*	(0.86)	(6.77)	(0.44)	(0.10)	(0.88)	(0.24)	(2.06)	(0.59)	(0.03)	*(0.13)*
B5	10.113	64.48	64.20	−150.87	−141.10	63.22	60.89	95.51	80.05	61.20	50.36	165.10	*155.65*
(1)	NA	NA	NA	NA	NA	NA	NA	NA	NA	NA	NA	NA	NA
B6	10.407	68.87	61.03	−150.70	−155.48	175.35	*145.49*	109.25	177.12	49.17	56.93	164.09	*151.83*
(1)	NA	NA	NA	NA	NA	NA	NA	NA	NA	NA	NA	NA	NA
B7	12.615	64.47	61.52	−152.62	−152.37	−178.69	*169.80*	99.13	110.77	175.10	174.40	165.04	*149.39*
(3)	(0.672)	(0.01)	(7.90)	(2.66)	(17.29)	(0.56)	*(0.09)*	(0.54)	(0.11)	(1.23)	(0.46)	(0.05)	(1.52)

*Mean energy (kcal/mol) of minimized structures, with standard deviations in parentheses.

[†]Mean values (and standard deviations) in degrees measured in structures after simulated annealing.

[‡]Mean values (and standard deviations) in degrees measured in structures after minimization. Values in italics are restraint violations.

[§]Numbers in parentheses indicate the number of structures observed for each conformation.

[¶]Conformation contained some structures that violated the given restraint, along with some that did not.

extensive analysis of the solution behavior of the trimannoside using solvated MD.

Solvated molecular dynamics

We began the solvated MD analysis by selecting a low-energy structure from the family of structures representing conformation B1. We found that if only minimal initial minimization was employed, II-III ω would sometimes undergo a transition from 180° to 60°, effectively converting B1 into B2. In all cases, once equilibration was complete (<100 ps), II-III ω remained fixed for the remainder of the simulation. This enabled us to conduct simulations for both B1 and B2, and we will hereafter discuss data from two such simulations: a 1000-ps simulation with II-III $\omega = 180°$ (B1) and a 900-ps simulation with II-III $\omega = 60°$ (B2). Selected trajectories from these simulations are displayed in Figs. 4 and 5.

In an attempt to compare the results of the MD simulations with the NMR data, we computed average values for experimentally restrained internuclear distances and dihedral angles from sets of 4000 and 3600 structures, respectively, produced over the course of the B1 and B2 simulations. In the case of heteronuclear couplings, instantaneous values of J were calculated from the ϕ dihedral angles using Eq. 3, and these values were averaged. In the case of internuclear distances, an inverse sixth power average was calculated from the instantaneous values. For slower transitions this should yield an approximate time average for the distances derived from NOESY data. For more rapid transitions, a calculation that includes both angular and r^{-3} averaging is more appropriate; however, in our case, the majority of the rapid fluctuations are small and are not likely to demand a more rigorous treatment. These averages are listed in Table 5, along with values for two individual structures that most closely matched the average structures of the ensembles representing conformations B1 and B2. Also shown are the restraints for these parameters derived from NMR experiments. These data show that unlike the values for the static models, the MD average values are within 0.05 Å or 5° of the experimental ranges for most parameters. The two exceptions are the negative distance restraints for d(II-H1, III-H6R) and d(II-H1, III-H5) (B1 only), the averages of which are significantly smaller than that allowed by the restraints. However, using estimates of noise levels in the DPFGSE NOESY spectra, we calculated
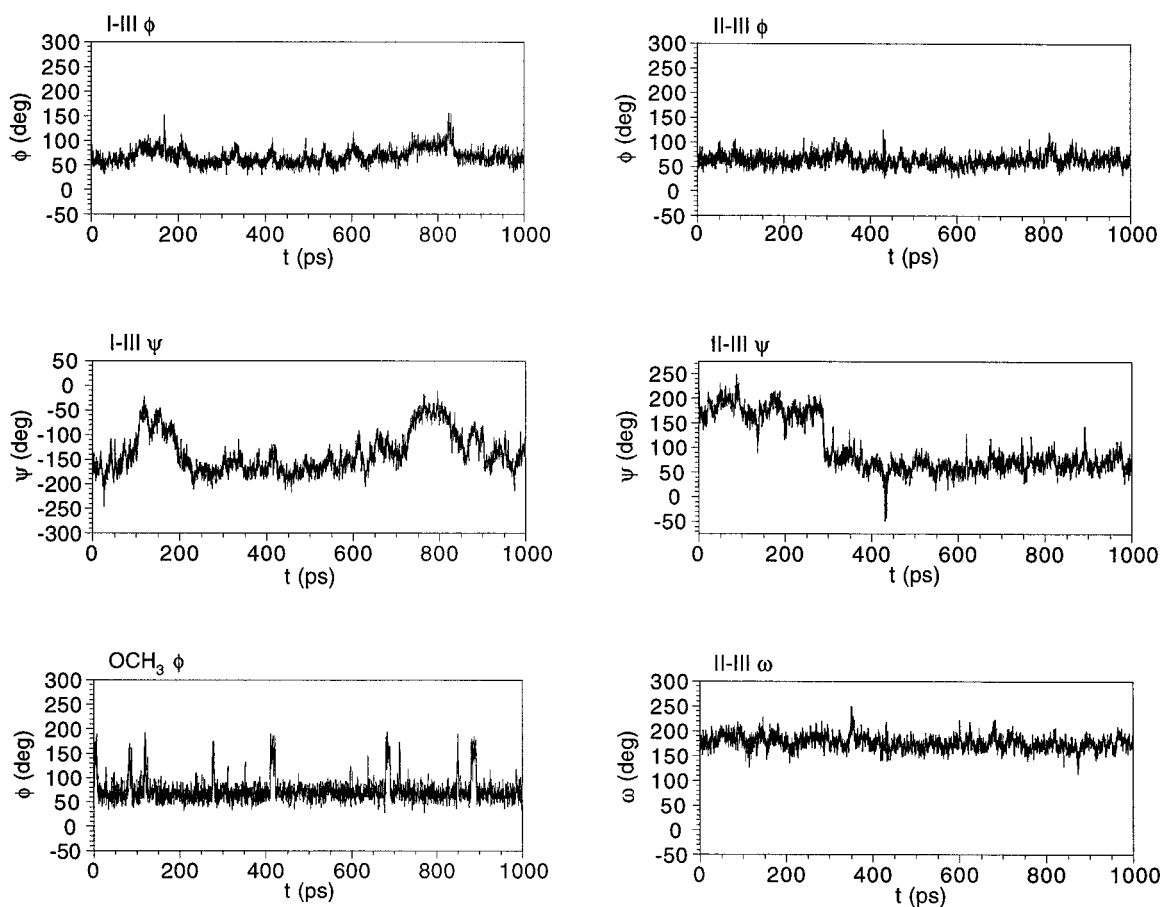

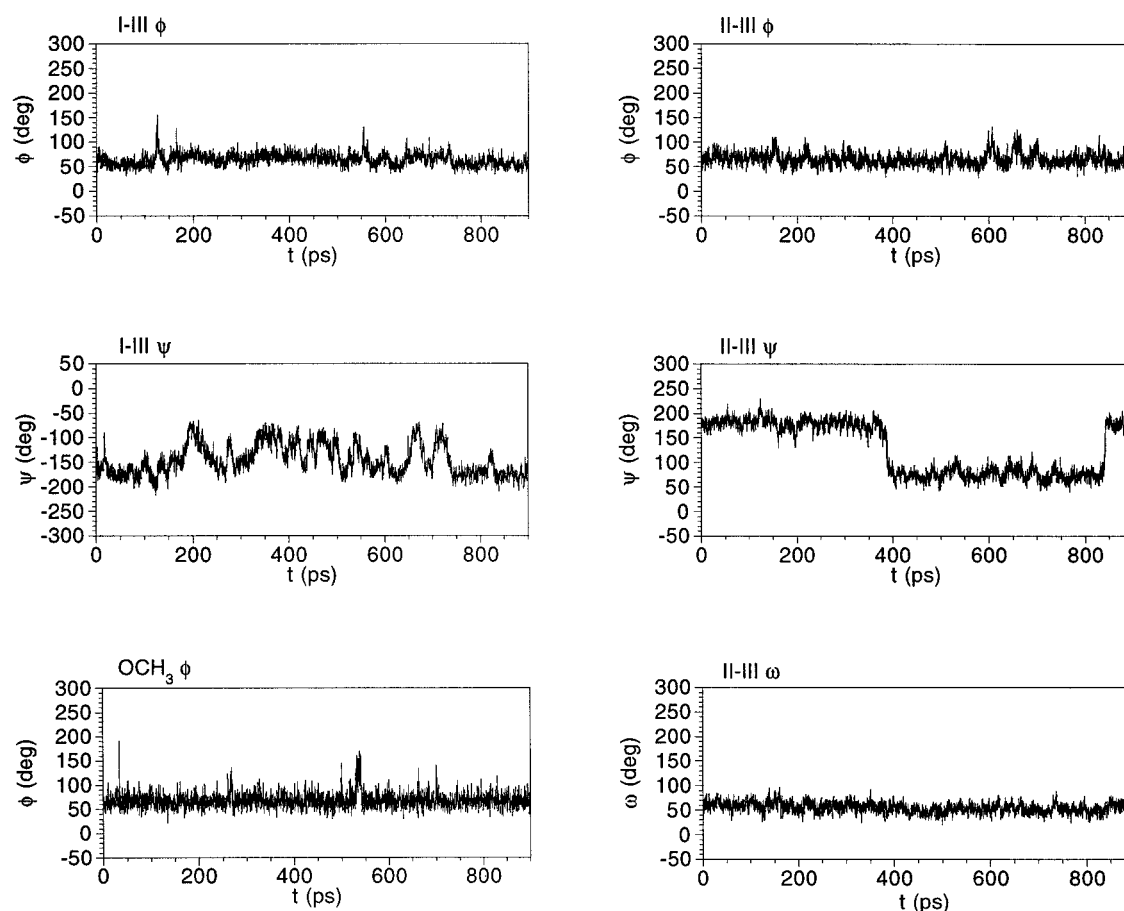FIGURE 4　MD trajectories for selected dihedral angles in conformation B1.

FIGURE 5   MD trajectories for selected dihedral angles in conformation B2.

minimum values for these distances that would allow an NOE to be observed and obtained values of 3.1–3.2 Å. Therefore, the MD averages for d(II-H1, III-H6R) are consistent with the NOESY data. As discussed below, the discrepancy in the average of d(II-H1, III-H5) may result from inadequate sampling of II-III ψ during the MD simulation. It thus appeared that as a whole, the MD simulation produced molecular behavior that is more consistent with the NMR data than either the static B1 or B2 models.

Preparation of a structural model

We now turn to the task of building a physical model of the structure or structures that the trimannoside samples in solution. We have divided this task into three parts: first, we seek to find a set of distinct structural conformations, each of which can be represented by a static structure; second, we seek to describe the inherent internal dynamics, or flexibility, of each conformation; and third, we seek to describe the kinetics of interconversion between these conformers. Our goal was to develop a model that placed all of the experimentally restrained parameters at values within the ranges of experimental error, which for all torsional and positive

distance restraints, corresponded to the ranges limited by $r2$ and $r3$ as shown in Table 5. We now shall discuss the results for each of the three glycosidic linkages separately, with the goal of producing the smallest set of distinct conformations that are consistent with the data.

OCH$_3$ linkage

We begin by considering whether or not the simplest model of a single, static conformation for this linkage is supported by the data. The first indication that such a simple model may be inappropriate was provided by the simulated annealing calculations. The fact that restraint violations only appeared after minimization suggests that the structures produced by simulated annealing may not have been local minima but were perhaps positioned in higher energy conformations by the imposed experimental restraints. From the data in Table 4, it is apparent that OCH$_3$ ϕ populated two states after simulated annealing (165 $\pm$ 1° and 70 $\pm$ 5°), both of which satisfy the restraint. After minimization, the latter state remained essentially constant, whereas the former decreased to ~150°, a value that does violate the restraint. The question raised is whether a finite population

TABLE 5 Summary of restrained structural parameters and their values in selected models

Parameter	B1 static	B1 MD average	B2 Static	B2 MD average	B1/B2 MD average*	Experimental range[†]
d(I-H1, III-H3)	2.94[‡]	2.51[¶]	2.87[‡]	2.51[§]	2.51[§]	2.26–2.46
d(I-H1, III-H4)	3.29	3.37	3.34	3.33	3.34	2.71–3.40
d(III-H2, I-H5)	2.74	2.62	2.73	2.56	2.58	2.57–2.67
d(II-H1, III-H6S)	2.51	2.67	2.50	2.55	2.58	2.47–2.61
d(II-H1, III-H6R)	2.94	3.31	2.87	3.14	3.19	(>) 4.00
d(II-H1, III-H5)	4.29	2.35	4.72	4.12	2.81	(>) 4.00
d(III-H1, OCH$_3$)	2.90	2.82	2.89	2.84	2.83	2.78–2.82
I-III ϕ	1.44[¶]	2.29[‖]	1.66[¶]	2.03[‖]	2.11[‖]	2.0–2.8
	57.6**	68.0[††]	60.5**	65.0[††]	65.9[††]	65–74[††]
II-III ϕ	1.94	1.95	2.25	2.17	2.10	1.2–2.0
	63.9	64.6	67.5	66.6	65.8	54–65
III-OCH$_3$ ϕ	1.90	2.48	1.98	2.32	2.37	2.1–2.9
	63.5	70.1	64.4	68.3	68.9	66–75

*Averages derived from a population weighted combination of the two MD trajectories as described in the text.
[†]Values (Å for distances, Hz for dihedral angles) indicate the extent of the flat energy well bottom of the penalty function ($r2 - r3$).
[‡]Values in Å measured from a static structure.
[§]$\langle r^{-6} \rangle^{-(1/6)}$ in Å calculated over the indicated MD trajectory.
[¶]$^3J_{CH}$ values in Hz calculated from Eq. 3.
[‖]Arithmetic mean $^3J_{CH}$ values in Hz calculated over the indicated MD trajectory.
**Values in degrees measured from a static structure.
[††]Values in degrees calculated from Eq. 3 nearest to the sampled MD values.

of the 150° state is supported by other data. We note that several brief transitions to this state occurred during the MD simulation, as shown in Figs. 4 and 5. Interestingly, all of these dynamics proceeded with no significant change in d(III-H1/OCH$_3$) (data not shown), rendering the NOESY experiments relatively insensitive to this motion. However, we note that $\phi = 64°$ corresponds to a J coupling of 1.95 Hz, which does not violate the restraint but nevertheless lies just outside of the experimental range (see Table 5). As $\phi = \sim150°$ corresponds to a J coupling of ~3.8 Hz, we would expect that the numerous, brief transitions observed would cause the average value of J to increase. Indeed, the static value of J is 1.9–2.0 Hz compared with the MD average values of 2.3–2.5 Hz, which agree very well with that measured experimentally. Moreover, we note that the MD average d(III-H1/OCH$_3$) values are slightly lower than those of the static models, bringing them into closer agreement with the experimental range (data not shown). It would thus appear that the presence of the $\phi = 150°$ state improves the agreement between the simulation and the experimental data. We can use measured and calculated J couplings to put an upper limit on the population of the $\phi = 150°$ state, and when we did this, we found that the population of this state must be less than 35%. In addition, from Table 4 we note that the 150° state, as seen in B4, imparts an energy penalty of ~2 kcal/mol in vacuo (compare B4 with B1), supporting only a minor population for $\phi = 150°$.

II-III linkage

Beginning with II-III ϕ, we found a pattern of results similar to that of OCH$_3$ ϕ. After simulated annealing, II-III ϕ

populated two states (58 ± 5° and 180 ± 5°), neither of which violated the restraint for this torsion. After minimization, the former state remained essentially the same, whereas the latter decreased to either 150° or 170°, both of which violate the restraint. The J values for the 150° and 170° states, which are 4.2 and 2.5 Hz, respectively, are both large compared with that experimentally observed and therefore can again be used to place upper limits on the populations of these states. If the 150° and 170° states were individually populated, these limits would be 5% and 15%, respectively. From Table 4, it is clear that both of these states, seen in B3 and B7, incurred energy penalties of at least 2 kcal/mol in vacuo. In addition, neither of these states was populated in either of the MD simulations, in which II-III ϕ remained predominantly near 64°. We thus concluded that II-III ϕ occupies primarily one state near 64°.

We next turn to II-III ψ and ω and begin by noting that the simulated annealing structures populated two states for each of these torsions. When II-III $\phi = 64°$, II-III ψ and ω each populated states near 180° and 60°. Likewise, in both MD trajectories (each corresponding to one of the II-III ω states), II-III ψ also sampled both the 180° and 60° states. Our task at this point was to find the minimum number of the four resulting (ψ, ω) states that are required by the data. Beginning with II-III ω, evidence regarding averaging at ω was obtained from the values of the proton homonuclear coupling constants between III-H5 and the two methylene protons of III-C6, as described by appropriate Karplus curves (Homans et al., 1986). For $\omega = 60°$, both $^3J_{5R}$ and $^3J_{5S}$ should be small, with values of ~2 Hz, but for $\omega = 180°$, $^3J_{5R}$ should be large (~11 Hz) although $^3J_{5S}$ remains at ~2 Hz. Clearly, the observed couplings for the triman-

noside (Table 1) are inconsistent with either of these values of ω being the sole state in solution. Therefore, we concluded that a single model for the II-III linkage is untenable and that averaging must take place at ω. Given the observed couplings and the average ω values from the two MD trajectories, a simple two-state calculation based on the Karplus curve predicted the population of $\omega = 180°$ to be 25–35% and that of $\omega = 60°$ to be 65–75%. It has been reported that the rates of ω transitions in solution are between 10^{-3} and 10^{-9} s^{-1} for D-mannose and D-glucose (McCain and Markley, 1987; Hajduk et al., 1993; Mäler et al., 1996) and are likely to be even slower when an additional pyranose ring is attached to the hydroxymethyl group (Brisson and Carver, 1983a). To simulate the averaging caused by the ω transition on the time scale of the NMR experiment, we combined the MD data from the two trajectories according to the populations predicted from the J couplings, and the resulting averages are also displayed in Table 5 as the B1/B2 MD average.

Given that averaging takes place at II-III ω, we next sought to determine whether averaging also takes place at II-III ψ. Although we have no torsional restraints for II-III ψ, the restrained distances at the II-III linkage are sensitive to the state of this torsion, as shown in Table 6. The only clear violation of the relevant restraints occurs in the (60°, 180°) state, which places d(II-H1, III-H5) at 1.87 Å. This short distance explains the small value of the B1 MD average for d(II-H1, III-H5), as the (60°, 180°) state is sampled for nearly 700 ps in the B1 trajectory. Moreover, it highlights a potential weakness of the MD simulations, in that II-III ψ underwent very few transitions over the course of the two simulations, indicating that this torsion may have been sampled insufficiently. This would cause the MD averages to be unreliable estimates of the behavior of this linkage on the time scale of the NOESY experiment. To gain insight into what ψ averaging is consistent with the NMR data, we conducted a simple 3D grid search in the populations of three of the states and computed $\langle r^{-6} \rangle^{(-1/6)}$ averages for each set of populations. We then collected those sets that satisfied all of the restraints. Two principal observations were gleaned from these calculations. First, the (60°, 180°) state was not populated in any of the collected sets, most likely because of its severe violation of the d(II-H1, III-H5) restraint. Second, the population of the (60°, 60°) state was found to be at least 20% but less than

50%. If these two observations are combined with the ω populations derived above, we would predict that the population of the (180°, 180°) state is near 30%, whereas those of the (180°, 60°) and (60°, 60°) states are each between 20% and 50%. However, the (60°, 60°) state was not sampled in the simulated annealing, and in vacuo simulations indicated that this state is 6–7 kcal/mol higher in energy than the other two states. Nevertheless, at least a minor population of the $\psi = 60°$ state is supported by the MD trajectories. Given all of the data, we therefore concluded that the II-III linkage exists in two major (ϕ, ψ, ω) states, (64°, 180°, 60°) and (64°, 180°, 180°), while also occasionally sampling a third, minor state, (64°, 60°, 60°).

I-III linkage

Although the data for the previous two linkages support a model in which these linkages populate multiple conformations in solution, the I-III linkage is unique in that all of the calculated structures in ensembles A and B populated generally the same states for these torsions. However, as noted above, the standard deviations for I-III ϕ and ψ were the highest of all the glycosidic torsions. In addition, members of several conformations, such as B1 and B2, violated the restraints for I-III ϕ and d(I-H1, III-H3), suggesting that a single structure may not be consistent with these restraints. Variability at this linkage was also observed in the MD simulations. Although ϕ remained relatively fixed at ~60°, ψ sampled a variety of values, spending significant time both near −180° and between −90° and −60°. In addition, there were a number of smaller transitions, many of which are correlated with small variations of ϕ. An explanation for this behavior would be that the energy surface of this linkage is rather flat with few if any deep minima, thereby allowing the torsions to explore a variety of values with little selectivity. A (ϕ, ψ) energy surface calculated using the same GLYCAM force field confirmed this suspicion. A broad energy valley extends roughly parallel to the ψ axis, from near (50°, −190°) to near (80°, −50°). Within this valley lie two broad minima, minimum A near (50°, −180°) and minimum B near (80°, −60°). These minima are separated by a region around (−50°, −110°), which is only 2–3 kcal/mol higher in energy.

We first asked if a single static model for this linkage could be found that was consistent with the NMR data. Beginning with a model in which ϕ is near 70°, we examined the torsional restraint on ϕ and three internuclear distance restraints that are sensitive to the state of this torsion. These are d(I-H1, III-H3), d(I-H1, III-H4), and d(III-H2, I-H5). Structural modeling indicated that when ϕ is fixed at 68°, d(I-H1, III-H3) falls within its experimental range only when $\psi > -130°$. However, d(I-H1, III-H4) does the same only when $\psi < -160°$, and d(III-H2, I-H5) only when $-155° < \psi < -145°$. This indicated that it is impossible to satisfy these three distance restraints simulta-

TABLE 6   Internuclear distances for (ψ, ω) states of the II-III linkage

ψ	ω	d(II-H1, III-H6S)	d(II-H1, III-H6R)	d(II-H1, III-H5)
180°	60°	2.44*	3.03	4.72
60°	60°	3.02	3.64	3.50
180°	180°	2.44	3.03	4.19
60°	180°	3.02	3.64	1.87

*Values in Å.

neously at $\phi = 68°$. If ϕ is increased, the required region for d(I-H1, III-H4) changes little, although the limiting value of ψ for satisfying the d(I-H1, III-H3) restraint decreases, narrowing the gap between the required ψ regions for d(I-H1, III-H3) and d(I-H1, III-H4). However, at the same time the ψ values of the required region for d(III-H2, I-H5) increase, further separating them from the required regions for the other two distances. We therefore concluded that no single (ϕ, ψ) state is capable of satisfying these restraints simultaneously and that the structural model for this linkage must at least include conformational averaging at ψ. We again note in Table 5 that the MD average values for d(I-H1, III-H3) agree significantly better with the NMR data than do those of the static models, and it is tempting to credit this improvement to the complex behavior of ψ in the simulations. Although such behavior may be realistic, our task at this point was to determine what modes of averaging were most consistent with the NMR data.

To assist us in evaluating various models in light of the requirements of the NMR data, we conducted grid searches as described in Materials and Methods, collecting all sets that satisfied the NMR experimental ranges shown in Table 5. Examination of the MD trajectories suggested that a four-state model should be considered in which ϕ and ψ each adopt two states. Given the broad, flat valley in the energy surface and the high frequency of conversions in the MD simulations, we allowed both ϕ and ψ to sample values that were normally distributed about two means. We ranked the sets that were consistent with the NMR data by their respective energies derived from the energy surface and collected those sets with energies less than 1 kcal/mol greater than that of the lowest energy set. These 41 sets clustered around a single solution in which primarily two (ϕ, ψ) states were populated: ($50 \pm 11°$, $-189 \pm 8°$) and ($82 \pm 3°$, $-104 \pm 9°$). The populations of these two states were 0.38 ± 0.06 and 0.56 ± 0.09, respectively. The former state lies within minimum A on the energy surface, whereas the latter lies on the gentle slope just above minimum B.

We now turn to a closer analysis of the MD trajectories for the I-III linkage. To aid in this, I-III (ϕ,ψ) scatter plots are presented in Fig. 6 for the two MD trajectories corresponding to II-III ω states of 60° and 180°. First, it is immediately obvious from these plots that the fluctuations of I-III ϕ and ψ are correlated with one another. The only other evidence of correlated motion we could find in the trimannoside can be seen by closely comparing the cloud of (ϕ, ψ) states for the two states of II-III ω. When $\omega = 180°$, this cloud accurately mimics the broad valley in the energy surface, extending from minimum A ($50°$, $-180°$) to minimum B ($80°$, $-60°$). However, when $\omega = 60°$ the cloud of populated states extends only to an area near ($80°$, $-90°$), so that minimum B itself is no longer populated. This suggests that the range of motion of the I-III linkage is correlated with the state of II-III ω. If we next superimpose the (ϕ, ψ) states of the 41 sets resulting from the grid search described
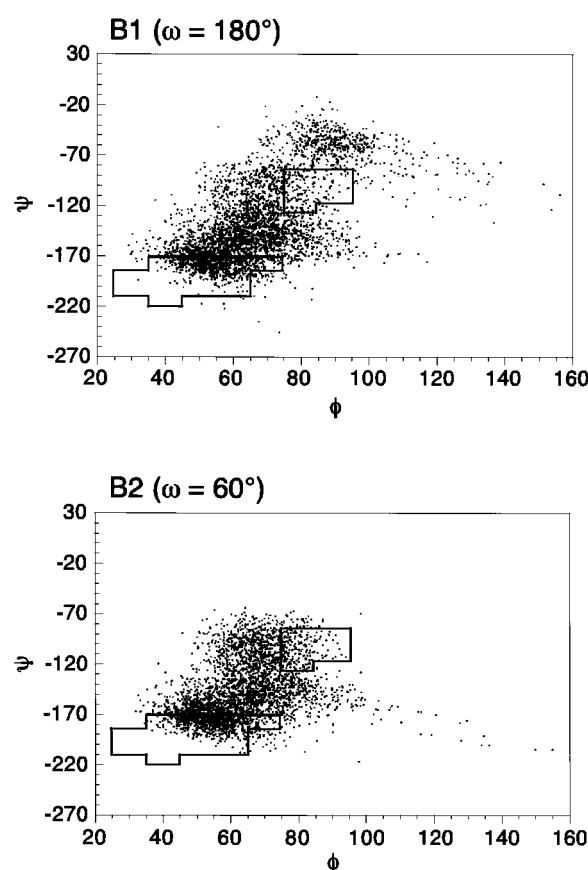

FIGURE 6 Scatter plots of the I-III ϕ and ψ trajectories from MD simulations for conformation B1 ($\omega = 180°$) and conformation B2 ($\omega = 60°$). Heavy lines enclose the ϕ and ψ values of states identified by grid searches as being consistent with the NOESY data.

above (enclosed by heavy lines) onto the population distributions observed in the MD, we find that the agreement is good, with areas of overlap centered near ($60°$, $-180°$) and ($80°$, $-100°$). We note that states in an area centered near ($70°$, $-140°$) as well as those near minimum B ($80°$, $-60°$) were populated in the MD simulation but were not included in models produced by the grid search. However, our models are consistent with some flexibility ($5-10°$) for ϕ and ψ, so we cannot rule out the occasional population of the ($70°$, $-140°$) or ($80°$, $-60°$) states. Moreover, given that our data indicate that the $\omega = 180°$ state is both the less populated of the two ω states and is correlated with the appearance of the ($80°$, $-60°$) state, this suggests that this latter state is minimally populated. What seems clear is that states near ($60°$, $-180°$) and ($80°$, -100°) were populated both in the MD simulations and in the grid search results and also lie within the broad energy minimum of the (ϕ, ψ) surface. Given that we desire to identify the minimum number of conformations required to fit our data, the ($60°$, $-180°$) and ($80°$, $-100°$) states seem to be the best candidates for these conformations. We therefore concluded that the behavior of the I-III linkage can be described by a model in which both

ϕ and ψ populate two states in a concerted manner, resulting in two major conformations: $(\phi, \psi) = (60°, -180°)$ and $(80°, -100°)$.

DISCUSSION

Description of the structural model

In summary, the data indicate that the trimannoside exists in solution as a molecule undergoing extensive conformational averaging. Such averaging occurs at all three glycosidic linkages, as summarized in Fig. 7. The dynamics are governed by five two-state transitions involving the following dihedral angles: I-III ϕ, I-III ψ, II-III ψ, II-III ω, and III-OCH$_3$ ϕ. The data indicate that the two transitions of the I-III linkage are correlated, and thus they are depicted as concerted transitions in our model, resulting in two (ϕ, ψ) states for the I-III linkage. In addition, the data indicate that a third state for this linkage, near minimum B, is correlated with the transition of II-III ω; however, as discussed above, the data suggest that the population of this state is small, and for simplicity it is not included in the model depicted in Fig. 7. We found no other correlated motions, and thus all other transitions are depicted as being mutually independent. These five transitions result in four major solution conformations (B1a, B1b, B2a, and B2b) and two minor conformations (B5a and B5b, both with II-III $\psi = 60°$). The

FIGURE 7 Structural model for the trimannoside in solution. The various transitions are labeled by the dihedral angle(s) involved, and for each angle the values of its two states are shown in degrees. Arabic numeral subscripts to the dihedral angles correspond to the glycosidic linkage (I-III, II-III). The structures are labeled according to the conformation observed in simulated annealing ensemble B (Table 4) having the equivalent states of the II-III linkage. The suffixes a and b differentiate the two states of the I-III linkage. For clarity, the transition involving III-OCH$_3$ ϕ is simply indicated by an arrow. All conformations shown place III-OCH$_3$ ϕ at 64°.
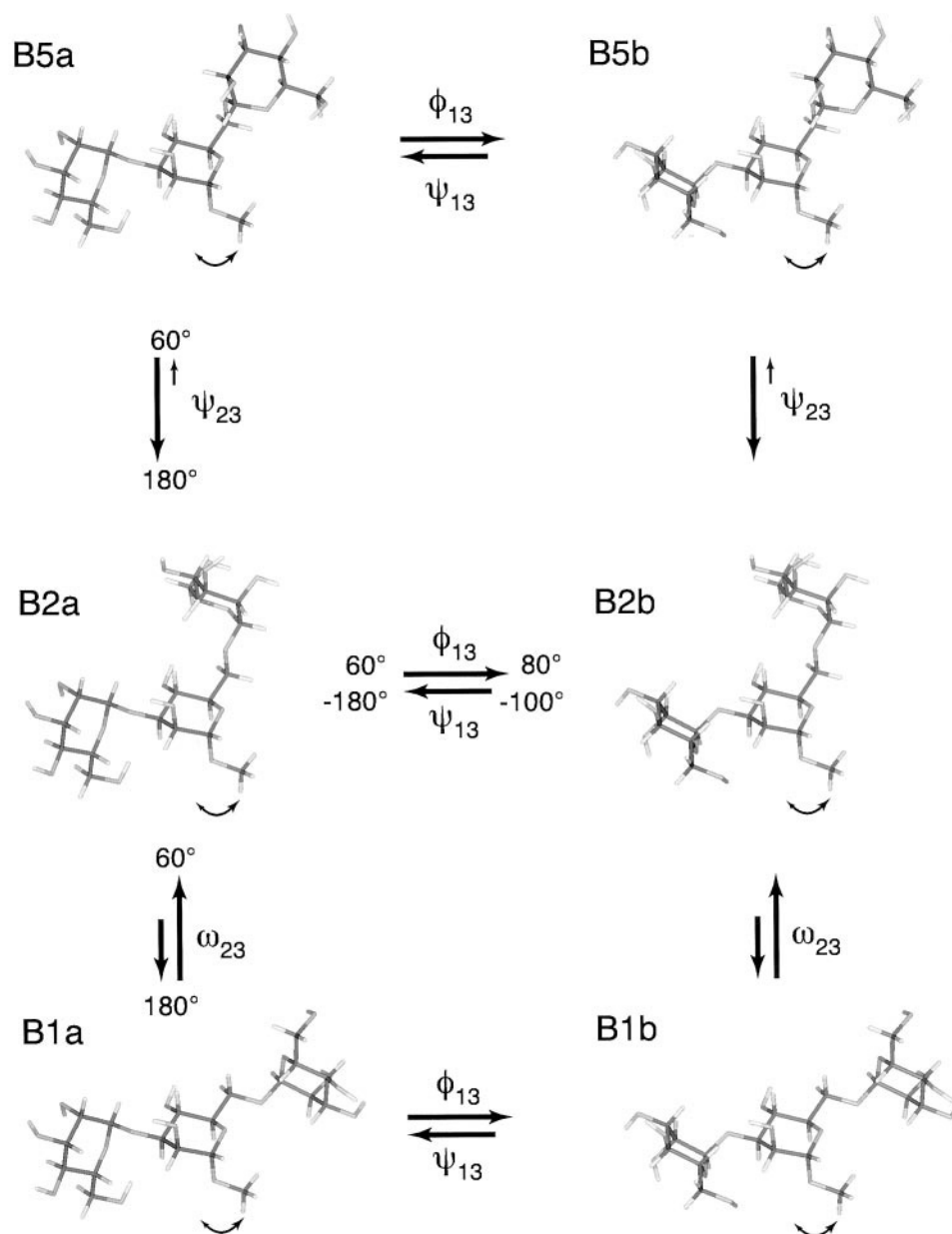
III-OCH$_3$ ϕ transition merely controls the placement of the terminal methyl group, and although it formally produces an additional set of six conformations, it has a very small effect on the overall molecular structure and is simply indicated by an arrow in Fig. 7. However, the other four transitions alter the relative orientations of the three mannose rings and thus could result in more profound changes in the molecular shape. This is most dramatically true for the transition of II-III ω, which interconverts the B1 and B2 conformations. As shown, for conformations with II-III $\psi = 180°$, when $\omega = 180°$ (B1a, B1b) the trimannoside is a roughly linear molecule, but when $\omega = 60°$ (B2a, B2b), the structure is bent by ~80° at the II-III linkage. In contrast, the transitions of the I-III linkage have relatively little effect on the molecular shape. Whereas this is not surprising for I-III ϕ, given the modest size of the transition (30°), I-III ψ has a substantial transition of 80°. Nevertheless, space-filling models of B1a and B1b show that both of them maintain essentially the same linear shape. The remaining transition, that of II-III ψ, takes place only when $\omega = 60°$ and thus modifies this bent structure. As shown, this transition rotates ring II away from ring I, effectively reducing the severity of the bend. Space-filling models of B5a and B5b confirm this and indicate that the bend is reduced to ~40°. Therefore, despite the complexity of the model presented in Fig. 7, the overall molecular structure of the trimannoside would appear to populate only three general topologies: a linear shape (B1: ψ, $\omega = 180°$, 180°), an occasionally populated, slightly bent shape (B5: ψ, $\omega = 60°$, 60°), and a severely bent shape (B2: ψ, $\omega = 180°$, 60°). As discussed previously, the available evidence further suggests that the dynamics of the II-III torsions are relatively slow, perhaps on a microsecond to millisecond time scale. This may well be a result of the large displacement of ring II and consequent solvent reorganization required to complete these transitions. On the other hand, the MD simulations would suggest that the dynamics of the I-III linkage are very rapid, with the individual conformations having lifetimes on the order of 100 ps. This behavior is consistent with the broad nature of the valley in the calculated energy surface for this linkage. Moreover, as these dynamics do not result in a significant change in the molecular shape, only minimal solvent reorganization should be required, allowing this portion of the molecule to exhibit rapid mobility.

Comparison to similar structures

Although past structural studies have concentrated on a wide variety of oligosaccharides containing the trimannoside or portions of it, relatively few have focussed on the trimannoside itself. One of the most thorough studies used steady-state NOE enhancements, proton and ^{13}C relaxation measurements, and potential energy calculations, and produced results that generally agree with those of the present study (Brisson and Carver, 1983a). Beginning with the

III-OCH$_3$ linkage, these authors noted a discrepancy in measured correlation times for the methyl group and postulated that this could arise from additional motions of this group that were not included in their treatment of the data. More recently, results of optical rotation studies on methyl α-D-mannopyranoside found that including a population of a $\phi = 180°$ state of 10–20% (in addition to the $\phi = 60°$ state) for the methoxy linkage was able to bring the calculated values of the molar rotation into agreement with those experimentally observed (Stevens et al., 1989; Stevens, 1994). These results agree well with our model, which supports a minor population of a $\phi = 150°$ state of less than 35%.

Considerable interest and debate has surrounded the conformation of the $\alpha(1\rightarrow3)$ linkage in mannose oligosaccharides for several years. In their study of the trimannoside, Brisson and Carver (1983a) found a (ϕ, ψ) state of (75° ± 10°, -135° ± 10°) and furthermore concluded that motional averaging was confined to a narrow range around this conformation. Moreover, Carver and co-workers found that this linkage adopted a similar state in a variety of other oligosaccharides (Brisson and Carver, 1983b; Cumming et al., 1986). In addition, MD simulations of several high-mannose oligosaccharides conducted in vacuo (Warin et al., 1979; Rao and Perlin, 1983) also found average states near (70°, -140°) for $\alpha(1\rightarrow3)$ linkages. However, other studies reported that the $\alpha(1\rightarrow3)$ linkage adopted a slightly different state near (100°, -90°) in a number of oligosaccharides (Homans et al., 1982, 1983, 1987a,b). Later studies using MD simulations, both in vacuo (Balaji et al., 1994) and including explicit solvent (Homans, 1990), along with other studies using proton relaxation measurements in partially deuterated samples (Hricovíni et al., 1992) all found evidence of internal motion at this linkage, suggesting that both of the previously identified states may be sampled in solution. More recent studies using optical rotation techniques (Stevens, 1994), molecular mechanics modeling (Dowd et al., 1995), and circular dichroism (Arndt and Stevens, 1996) have indeed concluded that states near (80°, -160°) and (80°, -80°) are likely to be equally populated in solution. These studies also predicted a small population (~10%) of a state near (160°, -80°). Concurring with these reports, our data exclude the possibility of a single state of ψ for the $\alpha(1\rightarrow3)$ linkage and are much better satisfied by two states of ϕ. Furthermore, the two states predicted by our model, (60°, -180°) and (80°, -100°), agree well with those mentioned above (Fig. 7), and our model also predicts that these two states are approximately equally populated. As shown in Figs. 4, 5, and 6, we found that this linkage did sample states near (160°, -80°) as well, although very briefly and only when $\omega = 180°$. Interestingly, the (75°, -135°) state originally proposed by Brisson and Carver is positioned almost precisely between the two states in our model. Indeed, using the parameters resulting from the grid search, the average (ϕ, ψ) state is (71°, -135°), whereas

that computed from the MD trajectories is $(67°, -137°)$. We also note that a recent study of the oligosaccharide $Man_9GlcNAc_2$, which contains two $\alpha(1\rightarrow3)$ linkages between mannose residues, found that one of these linkages also populates two conformations, and it was concluded that this was the result of the formation of a transient, inter-residue hydrogen bond (Woods et al., 1998). It would thus appear that the dynamic behavior of the $\alpha(1\rightarrow3)$ linkage can be complex, and is sensitive to its context in the overall oligosaccharide. Indeed, our data further suggest that the dynamics of this linkage in the trimannoside may be correlated with that of the $\alpha(1\rightarrow6)$ linkage in the molecule.

Turning now to the $\alpha(1\rightarrow6)$ linkage, Brisson and Carver reported the following dihedral angle values for the trimannoside: $\phi = 70° \pm 20°$, $\psi = 180°$, and $\omega = (180°, 60°)$. The two states of ω were found to be populated approximately equally and correspond exactly to those in conformations B1 and B2 in the present study. Although Brisson and Carver did not find a $\psi = 60°$ state, energy calculations were presented that showed a rather flat region for ψ ranging from 90° to 200° with a narrow minimum near 180°. Thus, a minor conformation with $\psi = 60–100°$ is perhaps consistent with such an energy surface. Our results also agree well with previous work on the $\alpha(1\rightarrow6)$ linkage in mannose oligosaccharides, a linkage that has been studied extensively (Brisson and Carver, 1983a,c; Homans et al., 1986; Cumming and Carver, 1987a,b; Balaji et al., 1994; Spronk et al., 1995; Taguchi et al., 1995). Although ϕ is typically found between 60° and 120°, ψ is often found to be variable, having multiple energy minima parallel to its axis on energy surfaces. Interestingly, potential energy calculations on methyl (6-O-α-D-mannopyranosyl)-β-D-mannopyranoside revealed that whereas the majority of molecules populated a $\psi = 180°$ state, a minor conformation with ψ near 90° was also produced, the population of which was dependent on the state of ω (Cumming and Carver, 1987a; Cumming and Carver, 1987b). Also, the recent study of $Man_9GlcNAc_2$ found that whereas ψ for one of the $\alpha(1\rightarrow6)$ linkages remained predominantly near 180°, it transiently populated a state of 90°, again due to the formation of an inter-residue hydrogen bond (Woods et al., 1998). Although no equivalent hydrogen bonds are possible in the trimannoside, it is notable that ring II has considerably more steric freedom relative to the corresponding internal residues in $Man_9GlcNAc_2$, and this may allow II-III ψ to sample the 60° state occasionally, as suggested by the former potential energy calculations. Finally, ω is found to be the most restricted dihedral angle, and populates some combination of the 60° and 180° states, the relative populations of which have a complex dependence on the presence of neighboring pyranose rings in the carbohydrate (Brisson and Carver, 1983c; Balaji et al., 1994; Taguchi et al., 1995). For instance, a recent study found that in methyl (6-O-α-D-mannopyranosyl)-α-D-mannopyranoside (the trimannoside without ring I), ω remained primarily in the 60° state

(Spronk et al., 1995). Our results confirm earlier studies and indicate that an additional mannose residue attached via an $\alpha(1\rightarrow3)$ linkage shifts the population distribution of ω to ~2:1 for the 60° and 180° states.

REFERENCES

Arndt, E. R., and E. S. Stevens. 1996. Experimental chiroptical verification of linkage flexibility in methyl 3-O-(α-D-mannopyranosyl)-α-D-mannopyranoside. *Biopolymers.* 38:567–571.

Balaji, P. V., P. K. Qasba, and V. S. R. Rao. 1994. Molecular dynamics simulations of high-mannose oligosaccharides. *Glycobiology.* 4:497–515.

Bax, A., and M. F. Summers. 1986. ^{1}H and ^{13}C assignments from sensitivity-enhanced detection of heteronuclear multiple-bond connectivity by 2D multiple quantum NMR. *J. Am. Chem. Soc.* 108:2093–2094.

Berendsen, H. J. C., J. P. M. Postma, W. F. van Gunsteren, A. DiNola, and J. R. Haak. 1984. Molecular dynamics with coupling to an external bath. *J. Chem. Phys.* 81:3684–3690.

Bevilacqua, M. P. 1993. Endothelial-leukocyte adhesion molecules. *Annu. Rev. Immunol.* 11:767–804.

Bolon, P. J., H. M. Al-Hashimi, and J. H. Prestegard. 1999. Residual dipolar coupling derived orientational constraints on ligand geometry in a 53 kDa protein-ligand complex. *J. Mol. Biol.* 293:107–115.

Brisson, J.-R., and J. P. Carver. 1983a. Solution conformation of αD(1–3)- and αD(1–6)-linked oligomannosides using proton nuclear magnetic resonance. *Biochemistry.* 22:1362–1368.

Brisson, J.-R., and J. P. Carver. 1983b. Solution conformation of asparagine-linked oligosaccharides: $\alpha(1–2)$-, $\alpha(1–3)$-, $\beta(1–2)$-, and $\beta(1–4)$-linked units. *Biochemistry.* 22:3671–3680.

Brisson, J.-R., and J. P. Carver. 1983c. Solution conformation of asparagine-linked oligosaccharides: $\alpha(1–6)$-linked moiety. *Biochemistry.* 22:3680–3686.

Cumming, D. A., and J. P. Carver. 1987a. Reevaluation of rotamer populations for 1,6 linkages: reconciliation with potential energy calculations. *Biochemistry.* 26:6676–6683.

Cumming, D. A., and J. P. Carver. 1987b. Virtual and solution conformations of oligosaccharides. *Biochemistry.* 26:6664–6676.

Cumming, D. A., D. S. Dime, A. A. Grey, J. J. Krepinsky, and J. P. Carver. 1986. Specific deuteration of a trimannoside confirms the existence of a disputed interresidue nuclear Overhauser enhancement. *J. Biol. Chem.* 261:3208–3213.

Davis, A. L., J. Keeler, E. D. Laue, and D. Moskau. 1992. Experiments for recording pure-absorption heteronuclear correlation spectra using pulsed field gradients. *J. Magn. Reson.* 98:207–216.

De Bruyn, A., and M. Anteunis. 1976. Conformation of the C-5/C-6 fragment of aldohexopyranoses. *Carbohydr. Res.* 47:311–314.

Dowd, M. K., A. D. French, and P. J. Reilly. 1995. Molecular mechanics modeling of α-(1-2)-linked, α-(1-3)-linked, and α-(1-6)-linked mannosyl disaccharides with MM3(92). *J. Carbohydr. Chem.* 14:589–600.

Drickamer, K. 1988. Two distinct classes of carbohydrate-recognition domains in animal lectins. *J. Biol. Chem.* 263:9557–9560.

Emsley, L., and G. Bodenhausen. 1990. Gaussian pulse cascades: new analytical functions for rectangular selective inversion and in-phase excitation in NMR. *Chem. Phys. Lett.* 165:469–476.

Ferrin, T. E., C. C. Huang, L. E. Jarvis, and R. Langridge. 1988. The MIDAS display system. *J. Mol. Graphics.* 6:13–27.

Gabius, H.-J. 1997. Animal lectins. *Eur. J. Biochem.* 243:543–576.

Hajduk, P. J., D. A. Horita, and L. E. Lerner. 201. 1993. Picosecond dynamics of simple monosaccharides as probed by NMR and molecular dynamics simulations. *J. Am. Chem. Soc.* 115:9196–9.

Heatley, F., L. Akhter, and R. T. Brown. 1980. Conformational analysis of appαricine using ^{1}H nuclear magnetic relaxation: application of transient nuclear Overhauser enhancements. *J. Chem. Soc. Perkin Trans. 2.* 1980: 919–924.

Homans, S. W. 1990. A molecular mechanical force field for the conformational analysis of oligosaccharides: comparison of theoretical and crystal structures of Manα1–3Manβ1–4GlcNAc. *Biochemistry.* 29: 9110–9118.

Homans, S. W., R. A. Dwek, J. Boyd, M. Mahmoudian, W. G. Richards, and T. W. Rademacher. 1986. Conformational transitions in N-linked oligosaccharides. *Biochemistry.* 25:6342–6350.

Homans, S. W., R. A. Dwek, D. L. Fernandes, and T. W. Rademacher. 1982. Solution conformation of the biantennary N-linked oligosaccharide of human serotransferrin using ^{1}H NMR nuclear Overhauser effect measurements. *FEBS Lett.* 150:503–506.

Homans, S. W., R. A. Dwek, D. L. Fernandes, and T. W. Rademacher. 1983. Solution conformation of biantenary complex type oligosaccharides: determination of major conformers about the glycosidic linkages. *FEBS Lett.* 164:231–235.

Homans, S. W., R. A. Dwek, and T. W. Rademacher. 1987a. Tertiary structure in N-linked oligosaccharides. *Biochemistry.* 26:6553–6560.

Homans, S. W., A. Pastore, R. A. Dwek, and T. W. Rademacher. 1987b. Structure and dynamics in oligomannose-type oligosaccharides. *Biochemistry.* 26:6649–6655.

Hricovíni, M., R. N. Shah, and J. P. Carver. 1992. Detection of internal motions in oligosaccharides by H-1 relaxation measurements at different magnetic fields. *Biochemistry.* 31:10018–10023.

IUPAC-IUB. 1983. Symbols for specifying the conformation of polysaccharide chains. *Eur. J. Biochem.* 131:5–7.

Krishnamurthy, V. V. 1996. Excitation-sculptured indirect-detection experiment (EXSIDE) for long-range CH coupling-constant measurement. *J. Magn. Reson. Ser. A.* 121:33–41.

Lasky, L. A. 1992. Selectins: interpreters of cell-specific carbohydrate information during inflammation. *Science.* 258:964–969.

Mäler, L., G. Widmalm, and J. Kowalewski. 1996. Motional properties of a pentasaccharide containing a 2,6-branched mannose residue as studied by ^{13}C nuclear spin relaxation. *J. Biomol. NMR.* 7:1–7.

McCain, D. C., and J. L. Markley. 1987. Internal motions of the three hydroxymethyl groups in aqueous sucrose. *J. Magn. Reson.* 73: 244–251.

Mohamadi, F., N. G. J. Richards, W. C. Guida, R. Liskamp, M. Lipton, C. Caufield, G. Chang, T. Hendrickson, and W. C. Still. 1990. MacroModel: an integrated software system for modeling organic and bioorganic molecules using molecular mechanics. *J. Comput. Chem.* 11:440.

Opdenakker, G., P. M. Rudd, C. P. Ponting, and R. A. Dwek. 1993. Concepts and principles of glycobiology. *FASEB J.* 7:1330–1337.

Oswood, M. C., Y. Kim, J. B. Ohlrogge, and J. H. Prestegard. 1997. Structural homology of spinach acyl carrier protein and *Echerichia coli* acyl carrier protein based on NMR data. *Proteins Struct. Funct. Genet.* 27:131–143.

Otter, A., R. U. Lemieux, R. G. Ball, A. P. Venot, O. Hindsgaul, and D. R. Bundle. 1999. Crystal state and solution conformation of the B blood group trisaccharide α-L-Fucp-(1→2)-[α-D-Galp]-(1→3)]-β-D-Galp-OCN3. *Eur. J. Biochem.* 259:295–303.

Pearlman, D. A., D. A. Case, J. W. Caldwell, W. S. Ross, T. E. I. Cheatham, D. M. Ferguson, G. L. Seibel, U. C. Singh, P. K. Weiner, and P. A. Kollman. 1995. A. M. B. E. R. 4.1. University of California, San Francisco.

Press, W. H., S. A. Teukolsky, W. T. Vetterling, and B. P. Flannery. 1992. Numerical Recipes in C. Cambridge University Press, New York.

Rance, M., O. W. Sorensen, G. Bodenhausen, G. Wagner, R. R. Ernst, and K. Wuthrich. 1983. Improved spectral resolution in COSY ^{1}H NMR spectra of proteins via double quantum filtering. *Biochem. Biophys. Res. Commun.* 117:479–485.

Rao, V. S., and A. S. Perlin. 1983. A reversal in the order of H-6R and H-6S chemical shifts of some aldohexopyranose derivatives, associated with the acetylation of OH-4 and OH-6 groups: a distinction between 3- and 4-linked D-glucose residues in disaccharides. *Can. J. Chem.* 61: 2688–2694.

Renouf, D. V., and E. F. Hounsell. 1995. Molecular modeling of glycoproteins by homology with non-glycosylated protein domains, computer simulated glycosylation and molecular dynamics. *In* Glycoimmunology. A. Alavi, and J.S. Axford, editors. Plenum Press, New York. 37–45.

Rundlof, T., A. Kjellberg, C. Damberg, T. Nishida, and G. Widmalm. 1998. Long-range proton-carbon coupling constants in conformational analysis of oligosaccharides. *Magn. Reson. Chem.* 36:839–847.

Rutherford, T. J., and S. W. Homans. 1994. Restrained vs free dynamics simulations of oligosaccharides: application to solution dynamics of biantennary and bisected biantennary N-linked glycans. *Biochemistry.* 33:9606–9614.

Rutherford, T. J., J. Partridge, C. T. Weller, and S. W. Homans. 1993. Characterization of the extent of internal motions in oligosaccharides. *Biochemistry.* 32:12715–12724.

Smith, S. A., T. O. Levante, B. H. Meier, and R. R. Ernst. 1994. Computer simulations in magnetic resonance: an object oriented programming approach. *J. Magn. Reson. Ser. A.* 106:75–105.

Spronk, B. A., A. Rivera-Sagredo, J. P. Kamerling, and J. F. G. Vliegenthart. 1995. A reinvestigation towards the conformation of methyl α-D-mannopyranosyl-(1-6)-α-D-mannopyranoside by a combined ROE and molecular dynamics analysis. *Carbohydr. Res.* 273:11–26.

Stevens, E. S. 1994. The potential-energy surface of methyl 3-O-(α-D-mannopyranosyl)-α-D-mannopyranoside in aqueous solution: conclusions derived from optical rotation. *Biopolymers.* 34:1395–1401.

Stevens, E. S., B. K. Sathyanarayana, and E. R. Morris. 1989. Optical rotation dispersion of saccharides: testing a theory. *J. Phys. Chem.* 93:3434–3436.

Stott, K., J. Stonehouse, J. Keeler, T.-L. Hwang, and A. J. Shaka. 2000. 1995. Excitation sculpting in high-resolution nuclear magnetic resonance spectroscopy: Application to selective NOE experiments. *J. Am. Chem. Soc.* 117:4199–4.

Taguchi, T., K. Kitajima, Y. Muto, S. Yokoyama, S. Inoue, and Y. Inoue. 1995. Proton NMR study of the trimannosyl unit in a pentaantennary N-linked decasaccharide structure: complete assignment of the proton resonances and conformational characterization. *Eur. J. Biochem.* 228: 822–829.

Tian, F., P. J. Bolon, and J. H. Prestegard. 1999. Intensity-based measurements of homonuclear residual dipolar couplings from CT-COSY. *J. Am. Chem. Soc.* 121:7712–7713.

Tolman, J. R., J. Chung, and J. H. Prestegard. 1992. Pure-phase heteronuclear multiple-quantum spectroscopy using field gradient selection. *J. Magn. Reson.* 98:462–467.

Tvaroska, I., M. Hricovini, and E. Petrakova. 1989. An attempt to derive a new Karplus-type equation of vicinal proton-carbon coupling constants for C-O-C-H segments of bonded atoms. *Carbohydr. Res.* 189:359–362.

van Halbeek, H. 1994. NMR developments in structural studies of carbohydrates and their complexes. *Curr. Opin. Struct. Biol.* 4:697–709.

Warin, V., F. Baert, R. Fouret, G. Strecker, G. Spik, B. Fouret, and J. Montreuil. 1979. The crystal and molecular structure of O-α-D-mannopyranosyl-(1→3)-O-β-D-mannopyranosyl-(1→4)-2-acetamido-2-deoxy-α-D-glucopyranose. *Carbohydr. Res.* 76:11–22.

Weis, W. I., G. V. Crichlow, H. M. K. Murthy, W. A. Hendrickson, and K. Drickamer. 1991. Physical characterization and crystallization of the carbohydrate-recognition domain of a mannose-binding protein from rat. *J. Biol. Chem.* 266:20678–20686.

Weis, W. I., K. Drickamer, and W. A. Hendrickson. 1992. Structure of a C-type mannose-binding protein complexed with an oligosaccharide. *Nature.* 360:127–134.

Willker, W., D. Leibfritz, R. Kerssebaum, and W. Bermel. 1993. Gradient selection in inverse heteronuclear correlation spectroscopy. *Magn. Reson. Chem.* 31:287–292.

Wishart, D. S., C. G. Bigam, J. Yao, F. Abildgaard, H. J. Dyson, E. Oldfield, J. L. Markley, and B. D. Sykes. 1995. ^{1}H, ^{13}C, and ^{15}N chemical shift referencing in biomolecular NMR. *J. Biomol. NMR.* 6:135–140.

Woods, R. J., R. A. Dwek, C. J. Edge, and B. Fraser-Reid. 1995. Molecular mechanical and molecular dynamical simulations of glycoproteins and oligosaccharides. I. GLYCAM 93 parameter development. *J. Phys. Chem.* 99:3832–3846.

Woods, R. J., A. Pathiaseril, M. R. Wormald, C. J. Edge, and R. A. Dwek. 1998. The high degree of internal flexibility observed for an oligomannose oligosaccharide does not alter the overall topology of the molecule. *Eur. J. Biochem.* 258:372–386.